Electromagnetic chirp of a compact binary black hole: A phase template for the gravitational wave inspiral

Zoltán Haiman

Phys. Rev. D **96**, 023004 — Published 14 July 2017

DOI: 10.1103/PhysRevD.96.023004

The electromagnetic chirp of a compact binary black hole: a phase template for the gravitational wave inspiral

Zoltán Haiman[1,21]

[11] *Department of Astronomy, Columbia University, 550 W. 120th St., New York, NY, 10027, USA*
[2] *Department of Physics, New York University, New York, NY 10003, USA*

The gravitational waves (GWs) from a binary black hole (BBH) with masses $10^4 \lesssim M \lesssim 10^7 \mathrm{M}_\odot$ can be detected with the *Laser Interferometer Space Antenna (LISA)* once their orbital frequency exceeds $10^{-4} - 10^{-5}$ Hz. The binary separation at this stage is $a = O(100)R_{\rm g}$ (gravitational radius), and the orbital speed is $v/c = O(0.1)$. We argue that at this stage, the binary will be producing bright electromagnetic (EM) radiation via gas bound to the individual BHs. Both BHs will have their own photospheres in X-ray and possibly also in optical bands. Relativistic Doppler modulations and lensing effects will inevitably imprint periodic variability in the EM light-curve, tracking the phase of the orbital motion, and serving as a template for the GW inspiral waveform. Advanced localization of the source by *LISA* weeks to months prior to merger will enable a measurement of this EM chirp by wide-field X-ray or optical instruments. A comparison of the phases of the GW and EM chirp signals will help break degeneracies between system parameters, and probe a fractional difference difference Δv in the propagation speed of photons and gravitons as low as $\Delta v/c \approx 10^{-17}$.

PACS numbers: 04.30.-w, 04.25.-g, 04.80.Cc

I. INTRODUCTION

Advanced LIGO has detected gravitational waves (GWs) from three stellar binary black hole (BBH) mergers, GW150914, GW151226, GW170104 [1–4] and measured the GW inspiral waveform over their last $\approx 5 - 30$ orbits. While no electromagnetic (EM) counterparts have been identified for these events, such counterparts could exist for stellar-mass BBHs embedded in dense gas, such as disks in active galactic nuclei (AGN) [5–7].

The space-based GW detector LISA [8] will be sensitive to supermassive BBHs in the range $10^4 - 10^7 \mathrm{M}_\odot$ and is expected to find dozens of merger events out to high redshifts ($z \sim 10$). These BBHs are produced in mergers of galaxies, which deliver the supermassive BHs, along with gas in the merging nuclei, to the center of the merger-remnant galaxy. The resulting compact BBHs are likely embedded in a gaseous environment, producing bright EM emission. Indeed, the abundance and redshift-evolution of bright quasars is comparable with the redshift-dependent rate of mergers, consistent with the idea that a significant fraction of quasars are trigged by such mergers [e.g. 9].

Identifying a GW source in EM bands would have considerable payoffs for cosmology and astrophysics [e.g. 10, 11]. Examples for cosmology include measurement of the Hubble constant [12], and probing gravity theories by comparing the luminosity-distance relation inferred from photons and gravitons [13]. Measuring the differences in the arrival times of photons and gravitons from the same cosmological source would be an independent test of the massive character of gravity and of possible violations of Lorentz invariance in the gravity sector [14].

In this paper, we focus on the last possibility. While previous work has suggested the idea of comparing the arrival times of photons and gravitons [e.g. 14–16], a crucial limitation has remained: in order to measure a difference in their propagation speeds, one needs to know when the photons vs. gravitons were emitted by the source. In general, this would require modeling the astrophysics of the source. Here we argue that for a compact massive BBH in the LISA band, such modeling is not required: as long as the EM photospheres envelope individual BHs (rather than the binary as a whole), the relativistic Doppler modulation from the orbital motion of the binary will inevitably imprint the analog of the GW chirp on the EM light-curve [17][18]. A measurement of this modulation of the EM light-curve will determine the absolute phase of the binary's orbit. Comparing the EM and GW chirp signals will help break degeneracies between system parameters, and will measure the relative propagation speed Δv of photons *vs* gravitons. Observing the same source with *LISA* and a wide-field X-ray (and possibly optical) instrument could probe a fractional difference as low as $\Delta v/c \approx 10^{-17}$.

II. PERIODIC ELECTROMAGNETIC EMISSION

EM emission from binaries – Recent hydrodynamical simulations have clarified the dynamics of a gaseous accretion disk around a BBH. Although the binary torques the inner disk and creates a low-density cavity, roughly twice the size of the binary separation, gas flows into this cavity through narrow streams [19]. Simulations in which the BHs are in the computational domain have furthermore shown that the individual BHs are fueled efficiently via their own "minidisks" [20–26]. This allows merging massive BHs to remain as bright as a typical quasar, nearly all the way to their merger [27].

EM emission from the BH components – The gas accreting onto each BH forms a minidisk extending out to

its tidal truncation radius. In units of their respective gravitational radii, these are $R_1/R_{g1} \approx 0.27q^{-0.3}(1+q)(a/R_g)$ and $R_2/R_{g2} \approx 0.27q^{-0.7}(1+q)(a/R_g)$ for the primary and secondary BH, respectively [28–30], where a is the binary's semi-major axis and R_g is the gravitational radius for the total mass. Simulations resolving the minidisks have found good agreement with these sizes [25]. The nature of the emission produced by accretion via each minidisk should resemble those from quasars.

In standard quasar accretion disk models, the EM emission is radially stratified, with high-energy radiation produced closer in. In a steady, Keplerian, optically thick disk around a BH of mass M, the thermal emission $\sigma_B T^4$ at radius R balances the local dissipation $3GM\dot{M}/8\pi R^3$, where T is the effective temperature at radius R, $\dot{M}$ the accretion rate, and G and σ_B are Newton's constant and the Stefan-Boltzmann constant [e.g. 31].

Integrating the black-body emission over the face of a disk with a temperature profile of $T \propto R^{-3/4}$, the surface brightness profile $I_\lambda(R) \propto [\exp((R/R_\lambda)^{3/4})-1]^{-1}$ has the scale radius at the observed wavelength λ_{obs}.

$$\frac{R_\lambda}{R_g} = 68 \left(\frac{\lambda_{obs}}{0.55\mu m}\frac{3}{1+z}\right)^{4/3} \left(\frac{M}{10^6 M_\odot}\right)^{-1/3} \left(\frac{\dot{M}}{\dot{M}_{Edd}}\right)^{1/3} . \quad (1)$$

Here $\dot{M}_{Edd} \equiv L_{Edd}/c^2$ is the accretion rate corresponding to the Eddington luminosity L_{Edd}, and we adopted a radiative efficiency of $\epsilon = 15\%$ and a quasar luminosity of $L = \epsilon \dot{M} c^2 = 0.15 L_{Edd}$. The fiducial wavelength of 0.55μm corresponds to the optical V band; in far UV bands ($\sim 0.15\mu$m) the disk would be ~ 5 times more compact ($R_\lambda \sim 12 R_g$). Note that $\approx 20\%$ of the total flux at λ_{obs} arises from inside the scale radius.

The X-ray emission observed from quasars is thought to arise from a combination of thermal disk emission and a hot corona. The size of the emitting region is limited by the broad observed FeKα line width and from variability measurements to be $\lesssim 10 R_g$ [32, 33]. The X-ray emission from a handful of quasars has been directly constrained via microlensing, with half-light radii consistent with this compact size [e.g. 34–37]. These X-ray-emitting regions fit around the individual BHs until the last stages of the merger, when the binary separation drops below $\lesssim 20 R_g$.

Microlensing observations in the optical band have found sizes consistent with eq. (1). However, the observed luminosities are significantly below the value predicted by the above simple model, and imply ~ 3 smaller disks (e.g. [38]). One resolution of this discrepancy is that the optical/UV radiation emerging from the inner disk is scattered at larger radii. For the compact binaries considered in this paper, the individual minidisks are truncated at $(10-30)R_g$. Reprocessing may then occur only by the narrow streams of gas inside the circumbinary cavity, with a small covering factor, and by the circumbinary disk farther out. We therefore consider the possibility below that the optical/UV emission is generated at radii ~ 3 times smaller than eq. (1).

Periodic relativistic modulation – The minidisks are fueled at a rate that varies periodically, on timescales comparable to the binary period [e.g. 20, 21, 25, 26, 39–44], which may introduce a corresponding periodic variation in the thermal EM emission [45]. However, for compact binaries at relativistic separations ($\beta \equiv v/c \gtrsim 0.1$, where v is the orbital velocity and c the speed of light), strong periodic variability is *inevitably* caused by relativistic Doppler modulation, and is expected to dominate the variability for mass ratios $q \equiv M_2/M_1 \lesssim 0.05$ [26]. The Doppler effect results from the orbital motion, and exists irrespective of the details of the emission.

Photons emitted by gas bound to individual BHs suffer a Doppler shift in frequency $D = [\Gamma(1-\beta_{||})]^{-1}$, where $\Gamma = (1-\beta^2)^{-1/2}$ is the Lorentz factor, $\beta_{||} = \beta \cos\phi \sin i$ is the component of the velocity along the line of sight, with i and ϕ the orbital inclination and phase. The apparent flux F_ν at a fixed observed frequency ν is modified from the flux of a stationary source F^0_ν to $F_\nu = D^3 F^0_{D^{-1}\nu} = D^{3-\alpha} F^0_\nu$. The last step assumes an intrinsic power-law spectrum $F^0_\nu \propto \nu^\alpha$. To first order in v/c, this causes a sinusoidal modulation of the apparent flux along a (circular) orbit, by a fractional amplitude $\Delta F_\nu/F_\nu = \pm(3-\alpha)(v/c)\sin i$ [46].

This Doppler modulation is a plausible explanation for the remarkably sinusoidal optical and UV light-curves of the bright $z = 0.3$ quasar PG 1302-102 [17], originally discovered by [47]. This quasar, with a 5.2 yr observed period ($a \sim 0.01$ pc ~ 300 R$_g$), is a mildly relativistic binary BH candidate with $v/c \sim 0.07$. For more compact binaries, additional general relativistic effects from time-delays and lensing will be important. While we do not consider these effects here, we note that they will enhance the periodic brightness modulations, while tracking the phase of the orbital motion [48].

As long as the BHs have their own photospheres, a periodic brightness modulation will be inevitable. The only exception would be the rare case of either (i) a face-on binary, or (ii) a widely separated equal-mass binary, inclined to the line of sight, for which the lensing effects are negligible, and the blue-shift/brightening of one BH cancels the red-shift/dimming of the other. In practice, a strict cancelation is unlikely, since any deviation from a pure power-law spectrum would result in asymmetric blue vs. redshift, even at $O(v/c)$.

III. ELECTROMAGNETIC CHIRP FOR BINARIES IN THE LISA BAND

LISA binaries – The key feature of the Doppler-induced periodic variability is that its phase tracks the orbit of the binary. For a massive BBH whose inspiral is detected by LISA, this phase can be compared directly with the evolving phase of the GW chirp signal. The GW

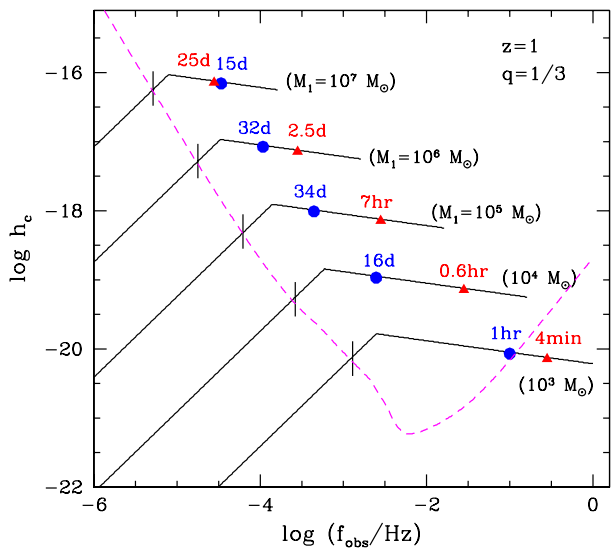

FIG. 1. *The figure shows the tracks across the LISA band of binaries at $z = 1$ with mass ratios of $q \equiv M_2/M_1 = 1/3$, and different primary masses M_1, as labeled. The break in the characteristic strain h_c marks 5 years prior to merger. Along each track, the marks correspond to the times when (i) the binary enters the LISA band (vertical line), (ii) the sky localization of a typical binary reaches an accuracy of 10 deg^2 (blue circle), and (iii) the tidal truncation radius of the circumprimary disk becomes smaller than $10R_{g1}$ (red triangle). The dashed (magenta) curve shows LISA's sensitivity, assuming a configuration with six links, 2 million km arm length, and a mission lifetime of five years [50]. Note that LISA is not planning to probe frequencies below 10^{-5}Hz, where the accelerometer noise is expected to rise steeply.*

frequency (twice the orbital frequency) is given by

$$f_{\rm GW} = 1.4\times10^{-4}\ {\rm Hz}\ \left(\frac{M}{10^6{\rm M}_\odot}\right)^{-1}\left(\frac{a}{60R_{\rm g}}\right)^{-3/2}. \quad (2)$$

The inspiral stage of a binary can be observed by LISA once its observed frequency enters the LISA band ($f_{\rm obs} = (1+z)^{-1}f_{\rm GW} \approx 10^{-4} - 10^{-5}$ Hz for $M = 10^4 - 10^7{\rm M}_\odot$). A compact binary will inspiral and merge, due to GW emission, on a timescale (to leading post-Newtonian quadrupole order; [49]) of

$$t_{\rm GW} = 0.17\ q_s^{-1}\ {\rm yr}\ \left(\frac{M}{10^6{\rm M}_\odot}\right)\left(\frac{a}{60R_{\rm g}}\right)^4, \quad (3)$$

where $q_s \equiv 4q/(1+q)^2$ is the symmetric mass ratio. Binaries can spend up to several years in the LISA band, and execute $\approx 1,900 q_s^{-1}(a/60R_{\rm g})^{5/2}$ cycles, over which the GW chirp is measured.

The evolution across the LISA band of binaries with mass ration $q = 1/3$, with several different primary masses (all at $z = 1$) is illustrated in Figure 1. The characteristic strain h_c, defined as the product of the sky- and polarization-averaged Fourier strain amplitude $h(f)$ and the square root of the number of cycles ($n_{\rm cycle} \equiv \min[f^2/\dot{f}, f\tau]$, where $\tau = 5$ years is the assumed LISA mission lifetime) is shown, along with the spectral noise density $S_{\rm n}(f)$. We adopted the LISA configuration with six links, 2 million km arm length, and $\tau = 5$yr (N2A2M5L6) from ref. [50].

Along each track we mark three characteristic times. (i) First, $q = 1/3$ binaries with primary masses $(10^7, 10^6, 10^5)$ M$_\odot$ enter the LISA band (defined as the time when the instantaneous S/N reaches $h_c/S_{\rm n} = 1$) when their separation is (62, 125, 253) $R_{\rm g}$, respectively (vertical marks). (ii) As the binary evolves and accumulates S/N, its parameters can be estimated to increasingly better accuracy. With the configuration we adopted, LISA can localize a typical $10^6{\rm M}_\odot$ binary on the sky to an accuracy of 10 deg^2 between a ∼week and a few months prior to the merger, with localization degrading rapidly with redshift, to ∼days at $z = 3$ [14, 51, 52]. The blue circle along each curve denotes the time when the localization error drops to 10 deg^2 for a typical binary. For simplicity, we assume that this occurs when the accumulated SNR reaches the value of S/N=50; this gives good agreement with the advance localization accuracies found previously in [14] and [51], who adopted a similar noise density (the accuracies vary by an order of magnitude, depending on the orientation of the orbital plane, spin magnitude and direction, and sky position). The advance localization is important for beginning an EM monitoring campaign, and occurs at separations of (18, 38, 68) $R_{\rm g}$. (iii) Finally, the red triangles denote the time when the tidal truncation radius of the circumprimary disk becomes smaller than $10R_{g1}$. Beyond this point the X-ray emitting regions are tidally stripped, and this occurs (25 days, 2.5 day, 7 hrs) prior to merger. Note that the typical 10^7 M$_\odot$ binary is localized too late, but the $(10^6, 10^5)$ M$_\odot$ binaries are localized well before this tidal stripping; they accumulate a total S/N=(195, 387) and complete (387, 2044) cycles between localization and tidal stripping. We list the evolution of binaries with a range of masses at $z = 1$ and 2 in Table 1. Although Doppler modulations from an equal-mass binary would cancel at $O(v/c)$ for a pure power-law spectrum, a precise cancelation is unlikely in practice: any asymmetry in the luminosities of the two BHs, and/or a departure from a pure power-law spectrum, would alleviate this cancelation. For illustration, we therefore include equal-mass binaries in Table 1, as well.

Measuring the EM chirp – The advance localization will allow pointing a wide-field telescope at the LISA error box and obtain a densely sampled EM light-curve, covering hundreds of cycles. We consider both X-ray and optical telescopes, but note that because of the tidal truncation discussed above, it is unclear if optical emission will still be present for a binary in the LISA band.

In the optical, for a $10^6{\rm M}_\odot$ BH at $0.5 < z < 3$, shining at the Eddington limit, the detection of 10% variability will require a sensitivity corresponding to 22-27 magnitudes [14]. As an example, the Large Synoptic Survey

Telescope (LSST; [53]) has a field of view (FOV) of 10 deg^2, which can cover the typical 2D sky localization error box from LISA, a month prior to merger, in a single pointing. LSST can reach a sensitivity of 27 mag (corresponding to a binary at $z = 3$) in an integration time of less than 1hr (see Table 1 in [14]). This is shorter than the orbital period and allows constructing a light-curve.

In the X-rays, as an example, the Wide Field Imager instrument on the proposed Athena mission [54] has a field of view of 0.5 deg^2 and an effective area of $\sim 1\mathrm{m}^2$ at 1keV. Tiling the full LISA error box a month before merger would require 20 pointings; alternatively, fewer cycles could be measured once the sky localization improves (an accuracy of 0.5 deg^2 will be available several days prior to merger [14, 51, 52]). The Lynx mission currently being developed [55] has a similar capability. For a $10^6\mathrm{M}_\odot$ BH at $z = 1$, with an X-ray luminosity of $L_X = 0.05L_{\rm Edd}$, Athena would collect ≈10 photons in a 10^3 sec integration, i.e. would obtain a flux measurement to $\sim 30\%$ accuracy throughout the 10 deg^2 area in ∼5 hrs. Continued tiling for a week would yield a measurement of ∼30 X-ray cycles throughout the field.

Once the periodic EM counterpart has been identified, the rest of a month-long monitoring campaign can focus on this source, and can be done by many other, smaller-FOV telescopes. We conclude that obtaining a well sampled EM light-curve should be feasible for binaries at $z = 1-2$ with masses $\mathrm{few}\times 10^3\mathrm{M}_\odot \lesssim M \lesssim \mathrm{few}\times 10^6\mathrm{M}_\odot$. Less massive binaries will have insufficient S/N, while more massive binaries enter the LISA band when their separation is already too compact for stable X-ray emission around the individual BHs (see Fig. 1 and Tab. 1).

IV. COMPARING THE ELECTROMAGNETIC AND GRAVITATIONAL WAVE CHIRP SIGNALS

Illustration – Figure 2 illustrates the comparison between the EM and GW chirp signals. The figure shows the strain from an edge-on ($\cos i = 0$), circular, $M_1 = 10^6\mathrm{M}_\odot$, $M_2 = 3\times 10^5\mathrm{M}_\odot$ binary at $z = 1$, with the chirp df/dt computed from the lowest-order PN (quadrupole) term. The corresponding EM light-curve is shown assuming a spectral slope $\alpha = -1$, modulated by relativistic Doppler boost at order v/c. We have furthermore assumed that the secondary BH out-accretes the primary, and is twice as luminous, based on the simulation results in [25]. Note that if the spectral slope α remains constant, the EM Doppler modulation amplitude ($v/c \propto f^{1/3}$) increases less steeply with frequency than the GW strain amplitude ($\propto f^{2/3}$). In principle, a few spectra, taken during the inspiral, could determine any evolution of α). The figure high-lights in blue the 387 cycles available for EM chirp measurement in X-rays, and possibly in other bands (see Table 1).

Figure 3 zooms in on the GW and EM chirp signals of the binary in Fig. 2, to show the few cycles around a look-back time of 32 days (when the binary is first

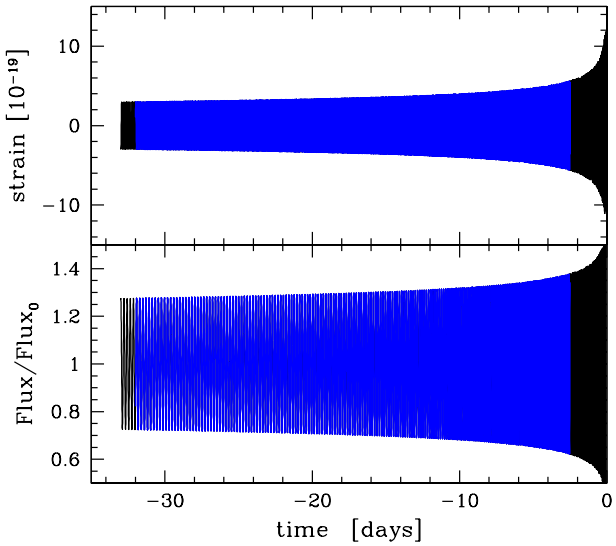

FIG. 2. *Illustration of the time-domain GW chirp and the EM light-curve for an $M_1 = 10^6$ M$_\odot$, $M_2 = 3\times 10^5$ M$_\odot$, circular, edge-on binary at $z = 1$. For clarity, the EM light-curve shows only the Doppler modulation and excludes lensing effects. The part of the signal shown in blue marks the ≈ 400 cycles available for EM chirp measurement in X-rays, and possibly in other bands. For this fiducial binary, the mean X-ray flux is $F_x = 0.05L_{\rm Edd}/4\pi d_L^2 = 2\times 10^{-15}$ erg s^{-1} cm^{-2}.*

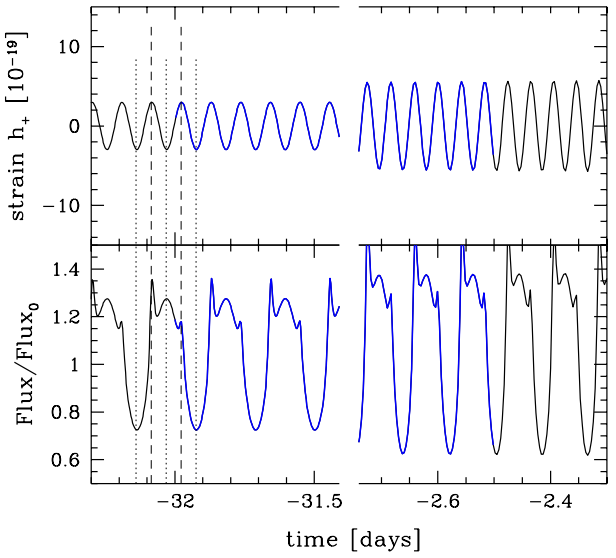

FIG. 3. *This figure zooms in on the GW and EM chirp signals of the binary in Fig. 2, to show the few cycles around a look-back time of 32 days (when the binary is first localized on the sky to 10 deg^2) and around 2.5 days (when the circumprimary disk is tidally stripped down to 10 $R_{\rm g1}$). The bottom panel assumes a tilt of the orbital plane 10° away from edge-on, to illustrate the asymmetric lensing of the primary and the secondary (the sharp peaks marked by the dashed lines).*

localized on the sky to 10 deg^2) and around 2.5 days (when the circumprimary disk is tidally stripped down to 10 $R_{\rm g1}$). In this figure, we have included the effect of gravitational lensing of whichever BH is behind the other, using the standard formula for lensing magnification to order v/c, $\mu = (x^2+2)/[x\sqrt{x^2+4}]$, where $x \equiv \theta/\theta_E$ is the angular distance between the two BHs on the sky, $\theta = \sqrt{(a\sin\theta)^2 + (a\cos\theta\cos i)^2}\, d_A^{-1}$, measured in units of the Einstein radius of the BH in the front, $\theta_E \approx 2(R_{\rm gi}a)^{1/2} d_A^{-1}$. Note that the effect is asymmetric; to show this asymmetry, we have assumed a small 10° tilt of the orbital plane away from edge-on ($i = 80$ deg).

Figure 3 shows several features of the correspondance between the time-domain GW chirp and the EM light-curve. First, in this example of a nearly edge-on binary, the GW is linearly polarized (h_+ only, $h_\times \approx 0$). The maxima of the GW strain correspond to the phase when the binary's axis is aligned with the line of sight. The Doppler modulation $\Delta F/F = (3+\alpha)v_{||}/c$ at this phase vanishes, however, this also coincides with the maximum lensing magnification. The Einstein radius for the primary is larger, causing a more pronounced brightening when the secondary is being lensed (marked by the left vertical dashed line), but the lensing of the primary is still visible (vertical dashed line on the right). The minima of the GW strain alternate to sample the maxima and minima of the underlying Doppler modulation of the EM light-curve (shown the three vertical dotted lines).

Clearly, the shape of the EM light-curve will depend on inclination and mass ratio (see also [56]). Larger inclinations would eliminate the lensing effect, but leave the phase of the EM chirp the same. On the other hand, the GW strain would acquire a cross-component ($h_\times \neq 0$) which is $\pi/2$ out of phase with the plus (h_+) component. Thus, comparing the EM and GW phases amounts to an independent measurement of the orbital inclination. Note that in our examples, the binary separation is $\gtrsim 20R_{\rm g}$, but for smaller separations, additional general relativistic effects, due to time-delay, and higher-order lensing, will become important [48]. The BH spins will also affect the modulation, especially in the case of unequal mass-ratio and precessing binaries.

Phasing accuracy – The signal-to-noise ratio ρ for measuring a deviation in the GW waveform is given by

$$\rho^2(\delta h) = 2 \times 4 \int_{f_{\rm min}}^{f_{\rm max}} df\, \frac{|\delta h(f)|^2}{S_n^2(f)} \qquad (4)$$

where $f_{\rm min}$ is the frequency when the observation begins (i.e. when the localization accuracy drops below 10 deg^2) and $f_{\rm max}$ is the frequency when the observation ends (i.e. when the tidal truncation radius of the primary BH drops below $10R_{\rm g1}$). The extra factor of two on the right-hand side is because of the assumed 3-arm configuration, equivalent to two independent interferometers. Because the EM chirp signal can provide a template for the phase evolution, we assume that these phases are precisely known, and evaluate the S/N for detecting a pure phase shift in the GW waveform, $\delta h = h(f)(1-\exp[i\Delta\psi(f)])$. Here $h(f) = \mathcal{A} f^{-7/6}\exp[i\psi(f)]$ is the frequency-domain inspiral waveform in the stationary-phase approximation, $\mathcal{A} = \pi^{-2/3}30^{-1/2}\mathcal{M}^{5/6}d_L^{-1}$ is the amplitude in the leading Newtonian order, $\mathcal{M} \equiv (M_1M_2)^{3/5}/(M_1+M_2)^{1/5}$ is the chirp mass, and d_L is the luminosity distance.

As a simple case, we consider a shift of the time-domain waveform by a constant Δt, $\delta h = h(f)(1-\exp[2\pi i f\Delta t])$. This depicts a constant propagation speed difference $\Delta v/c = c\Delta t/d_L$ of photons and gravitons, and yields

$$\rho^2(\delta h) = 16\int_{f_{\rm min}}^{f_{\rm max}} df\, \frac{|h(f)|^2[1-\cos(2\pi f\Delta t)]}{S_n^2(f)} \qquad (5)$$

$$\approx 8(2\pi\Delta t)^2 \int_{f_{\rm min}}^{f_{\rm max}} df\, \frac{|h(f)|^2 f^2}{S_n^2(f)}, \qquad (6)$$

where in the last step we assumed $2\pi f\Delta t \ll 1$. Fig. 1 shows that most of the signal-to-noise for $M \gtrsim 10^4$ M$_\odot$ is contributed near $f_{\rm max}$, at the highest frequency at which there is still X-ray emission. To a good approximation, a detectable shift corresponds to $\approx 10/\rho$ rad, for a source with overall signal-to-ratio ρ [57, 58]. Evaluating eq. (5) numerically, Table 1 lists the shift $\Delta v/c$ for each binary that would produce $\delta\rho = 10$. We find values as low as $\Delta v/c \approx 10^{-17}$.

If the velocity difference is due to gravitons with a nonzero mass m_g in a Lorentz-invariant theory [e.g. 59], then it will depend on frequency according to $\gamma m_g c^2 = h_p f$, where h_p is Planck's constant, f is the GW frequency, and γ the Lorentz factor for the graviton. If $m_g c^2 \ll h_p f$, the graviton speed differs from c by $\Delta v/c = 1/2(m_g c^2/h_p)^2 f^{-2} \propto f^{-2}$; this translates to a phase drift in the GW waveform $\Delta\psi(f) \propto f^{-1}$ [60]. In Table 1, we lists the graviton mass m_g for each binary that would produce $\delta\rho = 10$, computed with this phase drift, using eqs. 3.8 & 3.9 in [60]. We also list the equivalent Compton wavelength ($\lambda_g = h_p/m_g c$).

Although Lorentz invariance for photons has been tested to high accuracy, it could be violated in the gravity sector, especially over cosmological scales. This occurs, e.g. in brane-world scenarios with extra dimensions [e.g. 15, 16], or in vector-tensor scenarios [e.g. 61]; Lorentz-violating massive gravitons have also been proposed as candidates for cold dark matter [e.g, 62]. See refs. [57, 63] for in-depth discussions. Following the EM and GW chirp in tandem as they evolve over a decade in frequency would explicitly test whether any measured phase drift is consistent with the expectation from $\gamma m_g c^2 = hf$.

In principle, one should be able to tighten the above limits, by doing a direct cross-correlation analysis, or matched filtering, between the GW data stream and the light-curve of the EM counterpart(s). We also note that in case there are several variable quasars in the initial LISA error box, then this analysis will also help identify the correct counterpart to begin with (i.e. the object with period and phase closely matching those of the GWs).

Plasma effect for photons – The EM and GW signals can be offset from one another due to plasma effects slowing down the photons. The plasma frequency

		at localization				at tidal truncation					shift		
M_1	M_2	a	t_m	$f_{\rm min}$	$\Delta F/F_0$	t_m	$f_{\rm max}$	$\Delta F/F_0$	S/N	$N_{\rm cyc}$	$\Delta v/c$	$\log m_g$	$\log \lambda_g$
[$M_\odot$]	[$M_\odot$]	[$R_{\rm g}$]	[day]	[Hz]	%	[day]	[Hz]	%	-	-	[log]	[eV/c^2]	[km]
z=1													
10^3	10^3	190	23	-2.2	15	3min	-0.7	46	64	19670	-17.5	-24.0	15.1
10^4	10^4	99	17	-2.8	20	0.5hr	-1.7	46	530	3895	-18.2	-25.1	16.2
10^5	10^5	69	39	-3.6	25	0.2	-2.7		436	1510	-17.3	-25.8	16.9
10^6	10^6	35	26	-4.1	34	2.1	-3.7	46	214	232	-16.1	-26.3	17.4
3×10^6	3×10^6	24	18	-4.4	41	6.1	-4.2	46	87	58	-15.2	-26.3	17.4
10^7	10^7	16	12	-4.6	50	20	-4.7		–	–	–	–	–
10^5	3×10^4	68	34	-3.4	37	0.3	-2.5	69	387	2044	-17.4	-25.5	16.6
10^6	3×10^5	38	32	-4.0	50	2.5	-3.5	69	195	387	-16.1	-26.1	17.2
10^7	3×10^6	18	15	-4.5	74	25	-4.5	69	–	–	–	–	–
z=2													
10^5	10^5	41	7.8	-3.4	31	0.3	-2.9	46	177	385	-17.1	-25.5	16.6
10^6	10^6	22	6.6	-4.0	42	3.1	-3.9	46	60	37	-15.7	-25.8	16.9
3×10^6	3×10^6	16	4.7	-4.2	51	9.2	-4.3	46	–	–	–	–	–
10^5	3×10^4	40	5.9	-3.2	49	0.4	-2.7	69	145	456	-17.2	-25.2	16.3
10^6	3×10^5	24	7.7	-3.8	63	3.7	-3.5	69	56	57	-15.8	-25.7	16.8

TABLE I. *For binaries with different redshift, primary and secondary mass (M_1 and M_2; columns 1-2) the table shows the binary separation (a), time-to-merger (t_m), GW frequency ($f_{\rm min}$), and EM variability amplitude ($\Delta F/F_0 = (3+\alpha)v_{||}/c$ with $\alpha=-1$; we also assume that the less massive BH, or one of the equal-mass BHs, out-shines the other by a factor of two) when the binary is first localized to 10 deg^2 (assumed to coincide with S/N=50; cols. 3-6); the time-to-merger (t_m), GW frequency ($f_{\rm max}$), EM variability amplitude ($\Delta F/F_0$), S/N, and # of cycles accumulated since localization when the circumprimary disk is tidally truncated at $10R_{\rm g1}$ (cols. 7-11); and a constant velocity difference ($\Delta v/c$) or graviton mass (m_g) and equivalent Compton wavelength (λ_g) which could be measured to S/N= 10 (cols. 12-14).*

of the intergalactic medium is proportional to the density of free electrons, $n_e \approx 10^{-7}(1+z)^3{\rm cm}^{-3}$, yielding $\nu_p = (n_e e^2/\pi m_e)^{1/2} = 3$ Hz$(1+z)^{3/2}$, and the corresponding index of refraction $n = \left(1-\frac{\nu_p^2}{\nu^2}\right)^{1/2} \approx 1-10^{-34}\left(\frac{E}{1{\rm keV}}\right)^{-2}$. This shows that plasma effects for photons can become comparable to the $\Delta v/c$ measurement limit for radio waves with $\lambda \gtrsim 10$cm. This would become relevant in searching for periodic Doppler modulation of radio emission (e.g. from jets around the individual BHs, as proposed in [64]).

V. DISCUSSION AND CONCLUSIONS

Constraining the graviton mass by comparing the GW waveforms and the EM light-curves has been proposed previously in the context of compact white dwarf binaries [e.g. 65], and the possibility of an analogous measurement with massive BBHs was suggested by [14]. Here we followed up on the latter suggestion, and showed that the EM chirp signal, necessary to perform this experiment, will inevitably be produced by the relativistic Doppler modulations of the quasar-like emission from gas bound to the individual BHs. We also demonstrated that the EM chirp could be promptly (in a ∼week) identified by a wide-field X-ray telescope, a ∼month prior to merger, and would subsequently be available for monitoring for 2-3 weeks by other, smaller-field-of-view telescopes.

The EM chirp will serve as a template for the GW inspiral, allowing a novel test for theories with massive gravity or extra spatial dimensions. The constraints we find (Table 1) are ~ 4 orders of magnitude tighter than the current upper limit, 7.7×10^{-23} eV/c^2, from the LIGO waveforms [4]. They are comparable to the sensitivity that will be available from the phasing of GWs in LISA observations alone [57]. Compared to the latter forecasts, we have used only a restricted frequency-range, but have assumed that the EM template breaks degeneracies between the phase drift and other system parameters. Additionally, the EM chirp template should be useful in breaking parameter-degeneracies in the GW waveforms. As an example, the sky position is correlated with the orbital plane orientation; this degeneracy is broken by spin precession [51] and by higher harmonics [52], but only near the end of the inspiral, when these effects are large.

As the inspiral proceeds from a binary separation of $\sim 60R_{\rm g}$ to $20R_{\rm g}$, the minidisks surrounding each BH will gradually lose their outer annuli due to tidal stripping. Following the evolution of the luminosity and spectrum of the source, during this "peeling off" stage in the last few weeks of the inspiral, will provide a novel tomographic probe of the radial structure of the accretion disks.

We have conservatively focused here on the regime when the BHs are separated by $\gtrsim 20R_{\rm g}$, but the binary could possibly remain bright past this stage, and exhibit

periodic fluctuations even during its last ~ 10 orbits [e.g. 66, 67]. However, it is unclear whether the Doppler modulations, which arises from shocked gas near the binary but bound to individual BHs, can be as unambiguously related to the binary's orbital phase in this case as at the larger separations we discussed.

We have focused on the X-ray emission, but binaries may be bright at radio and gamma-ray energies (e.g. via Bremsstrahlung emission and/or via jets [64, 66]) all the way up to the merger. It may then be possible to discover the gamma-ray chirp signal without advance localization with an all-sky monitor. Barring this possibility, advance localization will be necessary for this experiment to work, and LISA would need to broadcast its data in real time.

While the gas accreting onto the BHs from a circumbinary disk can create bright quasar-like emission, it is unlikely to have an impact on the orbital evolution of the binary. When the binary is in the LISA band, and inspirals on time-scale of years, the gas torques are expected to be 4-5 orders of magnitude weaker [58, 68, 69].

Future work will need to develop the method proposed here, by taking into account effects we have neglected, such as the general relativistic modulations during the binary's orbit, using higher-order GW waveforms, as well as addressing the degeneracies between the full set of system parameters. The flux from quasars is known to vary stochastically, including quasi-periodic modulations in the X-rays bands. In the case of binaries, significant X-ray emission can arise from shocks in accretion streams and the circumbinary disk, which is likely to be modulated periodically. Such modulations can occur on the binary's orbital time, as well as on different timescales [30, 45]. While the periodic Doppler modulation is inevitable, the additional large fluctuations will constitute a noise. The uncertainty to which the periodic Doppler modulations can be extracted in the presence of this noise, perhaps via a cross-correlation or matched filtering analysis between the GW data stream and the EM light-curve, will need to be assessed in future work. Finally, the measurement errors of the EM light-curves, and on the absolute phase of the EM template, should be computed for specific future X-ray instruments.

ACKNOWLEDGMENTS

I thank Alessandra Buonanno, Csaba Csáki, Daniel Chung, Kohei Inayoshi, Feryal Ozel, Lorenzo Sironi, and Luigi Stella for useful discussions, and Daniel D'Orazio, Bence Kocsis and Geoffrey Ryan for useful comments on a draft of this manuscript. I also gratefully acknowledge support by a Simons Fellowship in Theoretical Physics (ZH) and by NASA grant NNX15AB19G.

[1] B. P. Abbott, R. Abbott, T. D. Abbott, M. R. Abernathy, F. Acernese, K. Ackley, C. Adams, T. Adams, P. Addesso, R. X. Adhikari, and et al., Physical Review Letters **116**, 061102 (2016), arXiv:1602.03837 [gr-qc].
[2] B. P. Abbott, R. Abbott, T. D. Abbott, M. R. Abernathy, F. Acernese, K. Ackley, C. Adams, T. Adams, P. Addesso, R. X. Adhikari, and et al., Physical Review Letters **116**, 241103 (2016).
[3] B. P. Abbott, R. Abbott, T. D. Abbott, M. R. Abernathy, F. Acernese, K. Ackley, C. Adams, T. Adams, P. Addesso, R. X. Adhikari, and et al., Physical Review X **6**, 041015 (2016), arXiv:1606.04856 [gr-qc].
[4] The LIGO Scientific Collaboration, the Virgo Collaboration, B. P. Abbott, R. Abbott, T. D. Abbott, F. Acernese, K. Ackley, C. Adams, T. Adams, P. Addesso, and et al., ArXiv e-prints (2017), arXiv:1706.01812 [gr-qc].
[5] J. M. Bellovary, M.-M. Mac Low, B. McKernan, and K. E. S. Ford, ApJ **819**, L17 (2016), arXiv:1511.00005.
[6] I. Bartos, B. Kocsis, Z. Haiman, and S. Márka, ApJ **835**, 165 (2017), arXiv:1602.03831 [astro-ph.HE].
[7] N. C. Stone, B. D. Metzger, and Z. Haiman, MNRAS **464**, 946 (2017), arXiv:1602.04226.
[8] P. Amaro-Seoane *et al.*, Proposal submitted to ESA (2017), arXiv:1702.00786 [astro-ph.IM].
[9] G. Kauffmann and M. Haehnelt, MNRAS **311**, 576 (2000), astro-ph/9906493.
[10] E. S. Phinney, in *The Astronomy and Astrophysics Decadal Survey* (2010) arXiv:0903.0098 [astro-ph.CO].
[11] J. S. Bloom *et al.*, in *The Astronomy and Astrophysics Decadal Survey* (2010) arXiv:0902.1527 [astro-ph.CO].
[12] B. F. Schutz, Nature **323**, 310 (1986).
[13] C. Deffayet and K. Menou, ApJ **668**, L143 (2007), arXiv:0709.0003.
[14] B. Kocsis, Z. Haiman, and K. Menou, ApJ **684**, 870-887 (2008), arXiv:0712.1144.
[15] C. Csáki, J. Erlich, and C. Grojean, General Relativity and Gravitation **33**, 1921 (2001), gr-qc/0105114.
[16] D. J. Chung, E. W. Kolb, and A. Riotto, Phys. Rev. D **65**, 083516 (2002), hep-ph/0008126.
[17] D. J. D'Orazio, Z. Haiman, and D. Schiminovich, Nature **525**, 351 (2015), arXiv:1509.04301 [astro-ph.HE].
[18] Ref. [70] considered a similar Doppler modulation that would arise following the tidal disruption of a star by a massive BBH at somewhat larger separations, but did not consider simultaneous direct measurement of GWs.
[19] P. Artymowicz and S. H. Lubow, ApJ **467**, L77+ (1996).
[20] J. Cuadra, P. J. Armitage, R. D. Alexander, and M. C. Begelman, MNRAS **393**, 1423 (2009), arXiv:0809.0311.
[21] C. Roedig, M. Dotti, A. Sesana, J. Cuadra, and M. Colpi, MNRAS **415**, 3033 (2011), arXiv:1104.3868 [astro-ph.CO].
[22] C. J. Nixon, P. J. Cossins, A. R. King, and J. E. Pringle, MNRAS **412**, 1591 (2011), arXiv:1011.1914 [astro-ph.HE].
[23] C. Roedig, A. Sesana, M. Dotti, J. Cuadra, P. Amaro-Seoane, and F. Haardt, A&A **545**, A127 (2012).
[24] R. Gold, V. Paschalidis, M. Ruiz, S. L. Shapiro, Z. B. Etienne, and H. P. Pfeiffer, Phys. Rev. D **90**, 104030 (2014), arXiv:1410.1543.
[25] B. D. Farris, P. Duffell, A. I. MacFadyen, and Z. Haiman,

ApJ **783**, 134 (2014), arXiv:1310.0492 [astro-ph.HE].
[26] D. J. D'Orazio, Z. Haiman, P. Duffell, A. MacFadyen, and B. Farris, MNRAS **459**, 2379 (2016), arXiv:1512.05788 [astro-ph.HE].
[27] B. D. Farris, P. Duffell, A. I. MacFadyen, and Z. Haiman, MNRAS **447**, L80 (2015), arXiv:1409.5124 [astro-ph.HE].
[28] B. Paczynski, ApJ **216**, 822 (1977).
[29] P. Artymowicz and S. H. Lubow, ApJ **421**, 651 (1994).
[30] C. Roedig, J. H. Krolik, and M. C. Miller, ApJ **785**, 115 (2014), arXiv:1402.7098 [astro-ph.HE].
[31] J. Frank, A. King, and D. J. Raine, *Accretion Power in Astrophysics, by Juhan Frank and Andrew King and Derek Raine, pp. 398. ISBN 0521620538. Cambridge, UK: Cambridge University Press, February 2002.* (Cambridge University Press, Cambridge, UK, 2002).
[32] C. S. Reynolds and M. A. Nowak, Physics Reports **377**, 389 (2003).
[33] G. Miniutti and A. C. Fabian, MNRAS **349**, 1435 (2004), astro-ph/0309064.
[34] X. Dai, C. S. Kochanek, G. Chartas, S. Kozłowski, C. W. Morgan, G. Garmire, and E. Agol, ApJ **709**, 278 (2010), arXiv:0906.4342 [astro-ph.HE].
[35] J. Jiménez-Vicente, E. Mediavilla, C. S. Kochanek, and J. A. Muñoz, ApJ **806**, 251 (2015), arXiv:1502.00394.
[36] G. Chartas, C. Rhea, C. Kochanek, X. Dai, C. Morgan, J. Blackburne, B. Chen, A. Mosquera, and C. MacLeod, Astronomische Nachrichten **337**, 356 (2016), arXiv:1509.05375 [astro-ph.HE].
[37] E. Guerras, X. Dai, S. Steele, A. Liu, C. S. Kochanek, G. Chartas, C. W. Morgan, and B. Chen, ApJ **836**, 206 (2017), arXiv:1609.05192 [astro-ph.HE].
[38] C. W. Morgan, C. S. Kochanek, N. D. Morgan, and E. E. Falco, e-print ArXiv:0707:0305 (2007).
[39] K. Hayasaki, S. Mineshige, and H. Sudou, PASJ **59**, 427 (2007), astro-ph/0609144.
[40] A. I. MacFadyen and M. Milosavljević, ApJ **672**, 83 (2008), astro-ph/0607467.
[41] S. C. Noble *et al.*, ApJ **755**, 51 (2012).
[42] J.-M. Shi, J. H. Krolik, S. H. Lubow, and J. F. Hawley, ApJ **749**, 118 (2012).
[43] D. J. D'Orazio, Z. Haiman, and A. MacFadyen, MNRAS **436**, 2997 (2013).
[44] J.-M. Shi and J. H. Krolik, ApJ **807**, 131 (2015), arXiv:1503.05561 [astro-ph.HE].
[45] B. D. Farris, P. Duffell, A. I. MacFadyen, and Z. Haiman, MNRAS **446**, L36 (2015), arXiv:1406.0007 [astro-ph.HE].
[46] For a circular orbit; non-sinusoidal modulations from eccentric orbits are easily incorporated into the analysis.
[47] M. J. Graham, S. G. Djorgovski, D. Stern, E. Glikman, A. J. Drake, A. A. Mahabal, C. Donalek, S. Larson, and E. Christensen, Nature **518**, 74 (2015), arXiv:1501.01375.
[48] J. D. Schnittman, T. Dal Canton, J. Camp, D. Tsang, and B. J. Kelly, ApJ, submitted; e-print ArXiv:1704.07886 (2017), arXiv:1704.07886 [astro-ph.HE].
[49] P. C. Peters, Physical Review **136**, 1224 (1964).
[50] A. Klein, E. Barausse, A. Sesana, A. Petiteau, E. Berti, S. Babak, J. Gair, S. Aoudia, I. Hinder, F. Ohme, and B. Wardell, Phys. Rev. D **93**, 024003 (2016), arXiv:1511.05581 [gr-qc].
[51] R. N. Lang and S. A. Hughes, ApJ **677**, 1184-1200 (2008), arXiv:0710.3795.
[52] S. T. McWilliams, R. N. Lang, J. G. Baker, and J. I. Thorpe, Phys. Rev. D **84**, 064003 (2011), arXiv:1104.5650 [gr-qc].
[53] See `www.lsst.org`.
[54] See `www.cosmos.esa.int/web/athena`.
[55] See `wwwastro.msfc.nasa.gov/lynx`.
[56] D.J. D'Orazio and R. Di Stefano, in preparation.
[57] C. M. Will, Living Reviews in Relativity **9**, 3 (2006), gr-qc/0510072.
[58] B. Kocsis, N. Yunes, and A. Loeb, Phys. Rev. D **84**, 024032 (2011), arXiv:1104.2322.
[59] S. F. Hassan and R. A. Rosen, Physical Review Letters **108**, 041101 (2012), arXiv:1106.3344 [hep-th].
[60] C. M. Will, Phys. Rev. D **57**, 2061 (1998), gr-qc/9709011.
[61] T. Jacobson and D. Mattingly, Phys. Rev. D **70**, 024003 (2004), gr-qc/0402005.
[62] S. L. Dubovsky, P. G. Tinyakov, and I. I. Tkachev, Physical Review Letters **94**, 181102 (2005), hep-th/0411158.
[63] E. Berti, A. Buonanno, and C. M. Will, Classical and Quantum Gravity **22**, S943 (2005), gr-qc/0504017.
[64] G. Kulkarni and A. Loeb, MNRAS **456**, 3964 (2016), arXiv:1507.06990.
[65] C. Cutler, W. A. Hiscock, and S. L. Larson, Phys. Rev. D **67**, 024015 (2003), gr-qc/0209101.
[66] T. Bode, R. Haas, T. Bogdanović, P. Laguna, and D. Shoemaker, ApJ **715**, 1117 (2010), arXiv:0912.0087 [gr-qc].
[67] D. B. Bowen, M. Campanelli, J. H. Krolik, V. Mewes, and S. C. Noble, ApJ **838**, 42 (2017), arXiv:1612.02373 [astro-ph.HE].
[68] Z. Haiman, B. Kocsis, and K. Menou, ApJ **700**, 1952 (2009), arXiv:0904.1383 [astro-ph.CO].
[69] Y. Tang, A. MacFadyen, and Z. Haiman, MNRAS, in press (2017), arXiv:1703.03913 [astro-ph.HE].
[70] K. Hayasaki and A. Loeb, Scientific Reports **6**, 35629 (2016), arXiv:1510.05760 [astro-ph.HE].